



# Reinforcing effects of fibrous and crystalline nanocelluloses on cellulose acetate membranes

Nasrin Attari<sup>a,b,\*</sup>, Robert Hausler<sup>a,b</sup>

<sup>a</sup> Department of Civil and Environmental Engineering, École de Technologie Supérieure University of Quebec, Montreal, Quebec H3C1K3, Canada

<sup>b</sup> La Station Expérimentale des Procédés Pilotes en Environnement (STEPPE-ÉTS, École de Technologie Supérieure), Montreal, Quebec H3C1K3, Canada

## ARTICLE INFO

### Keywords:

Nanocelluloses  
Cellulose acetate  
Composite electrospun nanofibers  
Mechanical properties  
Heat post-treatment  
TEMPO-Oxidized cellulose nanofibril  
Cellulose nanocrystal

### MSC:

0000  
1111

### PACS:

0000  
1111

## ABSTRACT

An innovative approach to selectively separating molecules and ions has been developed using polymer nanocomposite membranes that consist of a continuous polymer phase and a nanofiller phase. To address the challenges associated with filtration, we have developed and compared a nanofibrous cellulose acetate (CA)-based membrane reinforced with cellulose nanofibrils (CNFs) and cellulose nanocrystals (CNCs). Several parameters including the morphologies, chemical interactions, and mechanical properties of the membranes were investigated after they were synthesized using the electrospinning technique and after they were heat treated. The polymer solutions were composed of various weight percentages of CNCs, 2,2,6,6-tetramethyl-1-piperidinyloxy (TEMPO)-mediated oxidized CNFs (i.e., 0 wt% to 1 wt%), and 15 wt% of CA. Based on our study, the reinforcing properties of TOCNF nanofillers were superior to CNC nanofillers. Heat-treated 0.25TOCNF/CA composite nanofibrous membrane achieved maximum ultimate tensile strength and elongation at the breakpoint of 33.31 MPa and 1.8%, respectively. The process-structure-property relationships outlined in this study can facilitate the fabrication and application of electrospun nanocomposite membranes for the purification of water.

## 1. Introduction

### 1.1. Membrane technology role in water and wastewater treatment

Different industrial establishments (i.e., food, clothing, pulp, chemicals, etc.) discharge several types of wastewater of varying volumes and contamination levels. The cleaning efforts are generally differentiated by industry and contamination type (e.g., organic: agri-food industry versus inorganic: metal industry) (Nasir et al., 2019; Patterson, 1985). An overall worldwide assessment of the pollution control efforts of different industrial sectors shows that membrane-based filtration technologies can be used in water purification in the primary metallurgy, metal processing, petroleum sectors, etc. The size of the industry and its location for discharging wastewater (networked or off-grid) determine the most appropriate preventive measures, which include monitoring wastewater changes, reducing at the source, and/or using cleaning technologies such as chemical precipitation, adsorption, ion exchange, coagulation-flocculation, and membrane filtration (Quebec Ministry of the Environment, 1995; Wilderer, 2010).

In recent years, membrane technology has been employed for water

purification, wastewater treatment, and reprocessing polluted water (Kugarajah et al., 2021). Using high-performance materials, membrane technologies have found a broad range of applications in industry and human life (Fane et al., 2011). Due to their low cost and ease of processing, polymers are the most commonly used membrane materials. Other performance requirements must be considered, including selective permeation, mechanical strength, thermal properties, and physicochemical stability, before practical application of a membrane material (Pinnau and Freeman, 2000). Additionally, polymer-based nanocomposites, which comprise a polymer bulk phase (i.e., continuous phase) and a nanofiller phase (i.e., dispersed phase) provide a promising solution to take advantage of synergistic interactions between the polymer bulk and the nanofiller (Bay et al., 2020; Divya and Oh, 2022; Wen et al., 2019).

### 1.2. Mechanical characteristics of nanocomposite membranes

Cellulose acetate (CA) is one of the most abundant polymer resources, an ester derivative of cellulose, an essential ingredient of green plant cell walls, and also one of the most favorable biodegradable

\* Corresponding author.

E-mail address: [nasrin.attari.1@ens.etsmtl.ca](mailto:nasrin.attari.1@ens.etsmtl.ca) (N. Attari).

<https://doi.org/10.1016/j.carpta.2023.100281>

Received 21 October 2022; Received in revised form 20 December 2022; Accepted 2 January 2023

Available online 9 January 2023

2666-8939/© 2023 The Author(s). Published by Elsevier Ltd. This is an open access article under the CC BY-NC-ND license (<http://creativecommons.org/licenses/by-nc-nd/4.0/>).

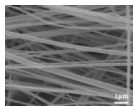
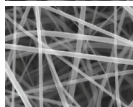
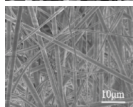
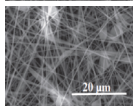
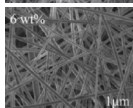
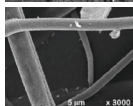
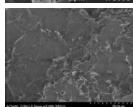
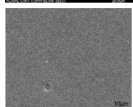
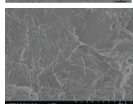
polymers for the preparation of polymeric membranes. The most common type of CA has an acetate group on two of its three hydroxyls (Babaei-Ghazvini and Acharya, 2022; Fischer et al., 2008; Jiang et al., 2020; Lee et al., 2018; Salama et al., 2018). CA-based membranes synthesized by electrospinning technique are widely used in filtration-based processes in particular water purification (Goetz et al., 2018; Voisin et al., 2017), wastewater treatment (Abdullah et al., 2019; Del Río De Vicente, 2021), biosensors (Vaidya and Wilkins, 1994), blood purification (Janeca et al., 2021), and tissue engineering (Stamatialis et al., 2008). This popularity originates from extensive bio-compatibility, biodegradability (Wsoo et al., 2020), nontoxic nature, good chemical, thermal (Etemadi et al., 2016), and mechanical properties and relatively low cost (Aboamara et al., 2019). CA as an excellent electrical conductor is ideal for electrospinning processing (Wsoo et al., 2020). CA electrospun nanofibrous membranes (ENMs) have a high specific surface area, uniform morphology, high interconnected porosity resulting in high permeability flux (Zhou et al., 2016), controllable thickness, high alignment of nanofibers (Aruchamy et al., 2018), and good mechanical

strength (Lee et al., 2018; Suja et al., 2017) in comparison to the membranes fabricated by other techniques (e.g., phase inversion method).

Mechanical characteristics of membranes play a significant role in the performance of pressure-driven water purification processes in terms of water flux and selectivity. When nanofillers like cellulose nanocrystals (CNCs) and cellulose nanofibrils (CNFs) are introduced to a CA polymer solution and heat post-treatment (HPT) is performed, the fiber linkages and mechanical properties can be improved (Jiang et al., 2020; Jonoobi et al., 2010; Voisin et al., 2017; Wsoo et al., 2020). CNCs and CNFs are renewable nanoparticles originating from cellulose and depending on the source and preparation process, their lengths may vary between 100 and 2000 nm, and diameters range between 2 and 20 nm. Chemical or enzymatic pre-treatments can be used for their preparation to greatly influence their characteristics (Goetz et al., 2018; Ma et al., 2014; Mokhena et al., 2018). The most important pre-treatments are TEMPO-mediated oxidation, mechanical refining, hydrolyzation, and carboxymethylation. The key point in 2,2,6,

**Table 1**

Recent experimental studies on the mechanical properties and the microstructure of polymeric nanocomposite membranes.

Material	Fabrication method	Cellulose function	Mechanical properties				Microstructure	Ref.
			NCs <sup>a</sup> loading (wt %)	UTS (MPa)	Strain at break (%)	Modulus (GPa)		
CNC/CA	Electrospinning	filler/matrix	0.105	5.72	2.47	–		Jiang et al. (2020)
CNC/CA			0.5	16.7	1.24	1.68		Sun et al. (2015)
CNC/PVDF <sup>b</sup>		filler	4	3.3	88.1	3e-3		Wang et al. (2019b)
CNC/PVDF			2	17.2	–	0.105		Lalia et al. (2014)
CNC/CH <sup>c</sup> -PEO <sup>d</sup>			6	5.76	8	2.45		Wang et al. (2019a)
CMC <sup>e</sup> /PLA <sup>f</sup>			1	3.75	20	–		Gaitán and Gacitúa (2018)
CNF/PLA	Extrusion		5	34.8	3	1.27		Ghasemi et al. (2018)
CNF/CA	TIPS	filler/matrix	5	65	–	2.5		Sharma et al. (2021)
CNF/CA	NIPS		5	47.6	2.5	2.7		Cindradewi et al. (2021)

<sup>a</sup> Nanocelluloses.

<sup>b</sup> Poly(vinylidene fluoride).

<sup>c</sup> Chitosan.

<sup>d</sup> Poly (ethylene oxide).

<sup>e</sup> Cellulosemicrocrystal.

<sup>f</sup> Poly(lactic acid).

6-tetramethyl-1-piperidinyloxy (TEMPO)-mediated oxidation is the negatively charged surface of the crystals and the fibrils. The individual fiber and crystal due to electrostatic repulsion forces can be stayed free and results in an improved dispersion (Levanic et al., 2020; Patiño Masó et al., 2019). Furthermore, in order to cross-link the CNCs and TEMPO-oxidized cellulose nanofibrils (TOCNFs) and improve the fibrous linkages, the HPT process is recommended. The number of fiber cross-links per fiber length is the prominent factor that highly affects the tensile strength and Young's modulus of CA nanocomposite ENMs (Liu and Tang, 2007).

The microstructure and nanofiller loading of polymeric nanocomposite membranes fabricated by different techniques are summarized in Table 1. These nanocomposite polymers exhibit enhanced mechanical properties (e.g., ultimate tensile strength, elongation at break, and Young's modulus) due to the reinforcing effects of CNC and CNF nanofillers. The CNC as a filler has been used for reinforcing CA (Jiang et al., 2020; Sun et al., 2015), Poly(vinylidene fluoride) (PVDF) (Lalia et al., 2014; Wang et al., 2019b), poly(lactic acid) (PLA) (Gaitán and Gacitúa, 2018), chitosan-poly(ethylene oxide) (CH-PEO) (Wang et al., 2019a). CNC-reinforced CA nanocomposite ENMs in the loading range of 0–1 wt% showed the optimal UTS of 5.72 MPa and 16.7 MPa for 0.105 wt% CNC/CA ENM (Jiang et al., 2020) and 0.5 wt% CNC/CA ENM (Sun et al., 2015), respectively. CNF filler has been successfully used to reinforce PLA (Ghasemi et al., 2018) and CA (Cindradewi et al., 2021; Sharma et al., 2021). TIPS and NIPS techniques were used to synthesize CNF-reinforced CA nanocomposite flat sheet membranes. Among the samples shown in Table 1, the optimal mechanical properties were achieved for films with a CNF/CA concentration of 5 wt %. The SEM micrograph of this sample, however, indicates a dense bulk structure making them incomparable to fibrous ENMs. In spite of the higher tensile strength of membrane mats fabricated by phase inversion, fibrous-structured electrospun membranes are more advantageous in separation processes because of their higher specific surface area and superior selective permeation.

In this study, CNC/CA and TOCNF/CA nanocomposite ENMs were rationally synthesized by electrospinning method. In the first step, CA nanofibrous membranes were electrospun to produce pristine membranes of CA. In the next step, CNC and TOCNF nanofillers were applied to spinning polymer solutions to synthesize composite nanofibers. The nanofibrous membranes were loaded with CNC and TOCNF nanoparticles to improve their mechanical properties. Various properties of the samples were investigated, including their microstructure,

morphologies, physical, chemical, and mechanical properties. This work maps the process-structure-property hierarchy of CA-based nanofibrous composite membranes. As shown in the schematic in Fig. 1, at the most general level, we consider the main polymer material, nanofillers, and the solvent. As the process level, we dissolved the polymer solution using the ultrasonication technique until the nanofillers were well dispersed and well distributed in the spinning solution. The membrane samples were then synthesized by electrospinning and their structure was investigated using a Scanning electron Microscope (SEM). Two nanofibrous and bead-formed microstructures are shown as possible example structures. As the property level, the synthesized sample were further characterized to determine the chemical properties, and mechanical properties using Fourier transform infrared spectroscopy (FTIR), and universal tensile testing, respectively.

This paper is structured as follows: The polymer materials and the details of methods for the preparation of composite polymer solution and synthesis of composite ENMs and HPT process are explained in Section 2. In Section 3, the effects of nanofiller loading and HPT process on the morphological structure and mechanical properties of ENMs are discussed. We also discussed the results of FTIR and tensile strength tests to find out the improvement of the mechanical properties of ENMs. Furthermore, a summary and conclusions of our findings are presented in Section 4.

## 2. Methods

### 2.1. Materials

Cellulose Acetate (CA, Mn=50000,  $\rho=1.3$  g/mL, and average degree of substitution, DS $\approx$ 1.2), received from Sigma-Aldrich Chemistry, was used as the matrix polymer. Freeze-dried powder TEMPO-oxidized cellulose nanofibrils (TOCNFs, 98 wt% dry powder) and freeze-dried powder cellulose nanocrystals (CNCs, 98 wt% dry powder), purchased from Cellulose LAB, Canada were used as nanofillers in the preparation of ENMs. Different volume ratios of N-dimethylformamide, DMF, and acetone, purchased from Fisher Chemical Co., were used as the solvent without further purification.

The characteristic properties of CNC and TOCNF and TEM images of these nanofillers are presented in Table 2 and Fig. 2, respectively. Degree of substitution (DS) which refers to the average amount of hydroxyl groups in repeating units that were substituted with carboxyl groups is determined by the ability to chemically modify the repeating unit and is

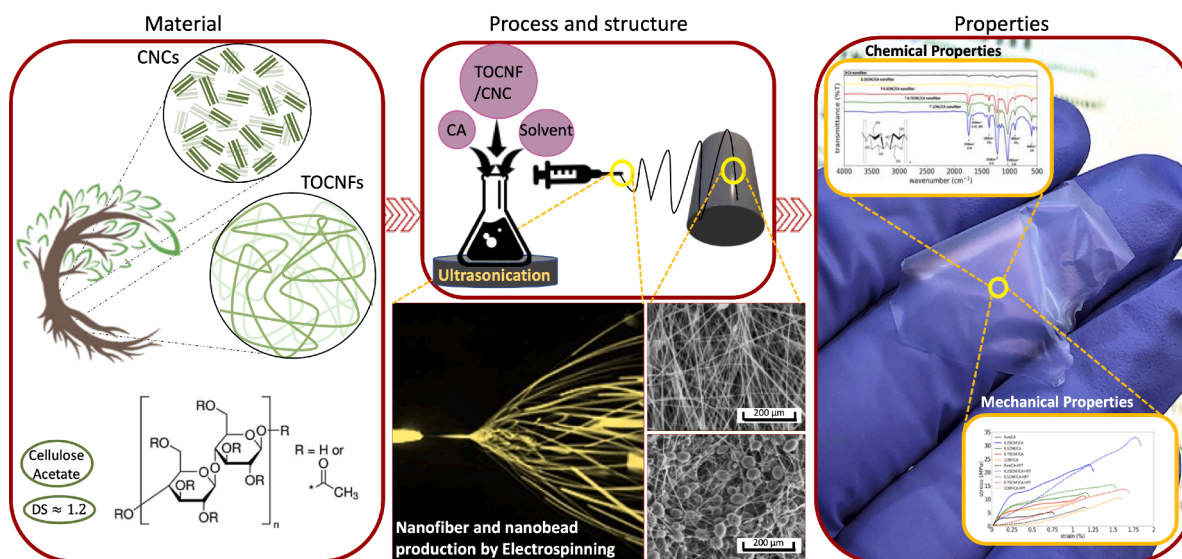


**Fig. 1.** Schematic representation of the material-process-structure-property chain in composite ENMs synthesized in this study. (left) Raw CA polymer; (middle) processing of the raw material and sample microstructure of obtained membranes; (right) A tiny membrane sample and the obtained representative properties.



**Table 2**

Properties of CNC and TOCNF nanofillers [Data courtesy of Cellulose LAB Company].

CNC properties	Units	Value
Degree of Substitution	%	5
Degree of Surface Substitution	%	>15
Content of Sulfate groups	g/100g CNC	0.8
Fiber Dimensions		width 5–20 nm, length 100–250 nm
TOCNF properties	Units	Value
Content of Carboxyl groups	mmol/g	1–1.2
Fiber Dimensions		width 50 nm, length 0.5–80 $\mu$ m

given in the table. The amount of carboxyl groups is determined by conductimetric titration of CNF after TEMPO-mediated oxidation using the curve of conductivity versus amount (mL) of added sodium hydroxide (Habibi et al., 2006). The content of sulfate groups, after hydrolysis, is determined by potentiometric titration. TEM images of TOCNF show a high degree of fibrillation, with diameters and lengths of a few micrometers. The TOCNF bundles form an entangled network. CNCs, on the other hand, have a cylindrical shape and are narrower (5–20 nm) and shorter (100–250 nm) because acid treatment dissolves the amorphous regions of the cellulose fibers, exposing the crystallites. Therefore, CNC has a lower aspect ratio than CNF.

## 2.2. Preparation of CNC/CA and TOCNF/CA composite polymer solutions

The polymer solutions were prepared by dissolving 15 wt% of CA in mixture solvent (volume ratio of 1:1) and dispersing different loadings of CNC or TOCNF nanofillers in a determined volume of acetone as described below. The calculated amount of CA, 7.5 gr, was stirred in half the volume of solvent for 24 h using a magnetic stirrer at 300 rpm at ambient temperature until the polymer was homogeneously dissolved. The CNCs or TOCNFs were first homogeneously dispersed in the calculated volume of acetone by magnetic stirrer for 24 h, followed by ultrasonication for 3 min. Then, a determined volume of DMF solvent was poured into NCs/acetone suspension and mixed for another 24 h. NCs/acetone-DMF suspension was then added to CA/solvent and stirred at 60 °C for an additional 12 h followed by ultrasonication for 3 min

until homogeneous dispersion of nanofiller was achieved. As outlined by Cindradewi et al. (2021) and Cai et al. (2019), NCs in the loading range of 0 wt% to 1 wt% can be well-dispersed in the spinning solutions especially at the lower loadings in accordance with the above-described methodology.

Table 3 summarizes the detailed sample codes, the values of nanofiller loading, and the implementation of the HPT process in the synthesis process. The samples were named as xCNC/CA where x represented the amount of CNC or TOCNF in the nanocomposite ENMs.

## 2.3. Electrospinning process

The preparation procedure of polymer solutions and the electrospinning process of CA ENMs were described in the previous work (Attari and Hausler, 2020). The set-up consists of a 20 mL BD plastic syringe as the solution container which is connected to a nozzle with an inner diameter of 0.8 mm to form the fibers. A pump controls the feed rate of the solution. The produced nanofiber samples are collected using a collector that is covered with aluminum foil to facilitate the peeling off the membrane from the collector. Furthermore, a power supplier (0–40 kV) is used to make the spinneret and the collector as two electrodes to provide electrostatic force to form the nanofibrous membrane samples. CNC/CA and TOCNF/CA composite spinning solutions with 15 wt% CA and variable CNC and TOCNF loadings were prepared. To achieve maximum efficiency, different loadings of CNC and TOCNF were added to previously obtained optimum solvent composition (Attari and Hausler, 2020). The composition of the optimum solvent is a dissolution of 15 wt% CA polymer in the equal volume ratio (1:1) of N, N-dimethylformamide (DMF), and acetone mixture solvent. All CNC/CA and TOCNF/CA ENMs were synthesized under previously obtained optimum electrospinning process parameter conditions: a polymeric solution flow rate of 2 mL/h, a distance between spinneret tip and collector (TCD) of 100 mm, an electric voltage of 25 kV and an electrospinning process time of 2 h (Attari and Hausler, 2020). The electrospinning process was performed in a temperature range from 20 to 26 °C and humidity range from 30 to 51%.

## 2.4. Optimization of the material and electrospinning process parameters

In our previous work (Attari and Hausler, 2020), the polymer solutions of various compositions of the solvent and CA concentrations were

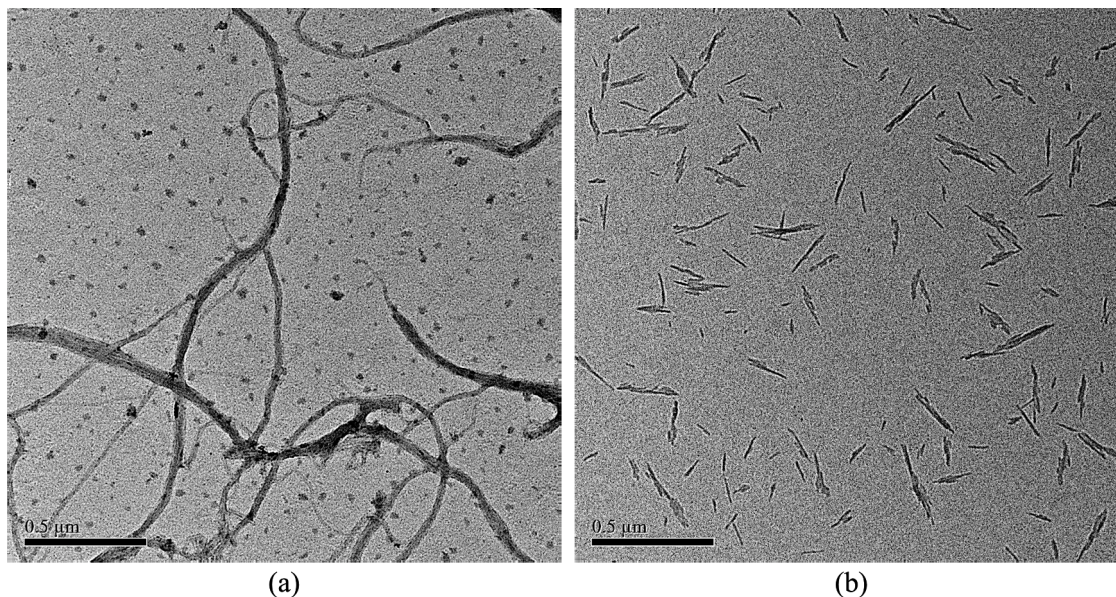


Fig. 2. TEM images of a) TOCNF and b) CNC [Image courtesy of Cellulose LAB Company].



**Table 3**  
The composition and formulation of synthesized nanocomposite ENMs.

Sample code	CA Concentration (wt%)	CNC Loading (wt%)	TOCNF Loading (wt %)	HPT Process
CA	15	0		×
CA-HPT	15	0		✓
0.25CNC/CA	15	0.25		×
0.25CNC/CA-HPT	15	0.25		✓
0.5CNC/CA	15	0.5		×
0.5CNC/CA-HPT	15	0.5		✓
0.75CNC/CA	15	0.75		×
0.75CNC/CA-HPT	15	0.75		✓
1CNC/CA	15	1		×
1CNC/CA-HPT	15	1		✓
0.25CNF/CA	15		0.25	×
0.25CNF/CA-HPT	15		0.25	✓
0.5CNF/CA	15		0.5	×
0.5CNF/CA-HPT	15		0.5	✓
0.75CNF/CA	15		0.75	×
0.75CNF/CA-HPT	15		0.75	✓
1CNF/CA	15		1	×
1CNF/CA-HPT	15		1	✓

prepared. Their morphological structure was studied to determine the optimized material and electrospinning process parameters. For the solvent composition, three-volume ratios of DMF and acetone, (2:8), (1:1), and (1:0) were intended. In the case of a volume ratio of (2:8), due to the high volatility of acetone, the needle tip was blocked during the electrospinning. For the volume ratio of (1:0), pure DMF, the high surface tension of this solvent resulted in the beads during the electrospinning process. According to the morphological results, by increasing the CA concentration from 10 wt to 15 wt%, the bead formation declined due to the increase in solution viscosity and surface tension. On the other hand, the further increase in CA concentration to 20 wt% increased the viscosity of the solution and made nanofiber formation more difficult. Therefore, the CA concentration of 15 wt% and (1:1) solvent ratio of DMF and acetone were determined to prepare polymer solutions for this study. The efficient values for process parameters were determined in regard to morphological study in our previous work. The electrospinning process parameters values such as voltage, polymer solution feed rate, tip to collector distance (TCD), and process time were kept constant at 25 kV, 2 ml/h, 100 mm, and 2 h, respectively.

### 2.5. Heat post treatment of CNC/CA, TOCNF/CA composite nanofibers

The loose and fluffy texture of the ENMs makes it difficult to handle them after the fabrication step. HPT process was conducted to improve the coherence structure and mechanical resistance of the CNC/CA and TOCNF/CA ENMs. HPT process was carried out in a glass beaker that contained deionized (DI) water at 70 °C which must be higher than the boiling point of the solvent mixture in order to complete evaporation of the solvent from the synthesized ENMs and lower than the glass transition temperature of the CA matrix polymer (110 °C) to form good connectivity between the nanofibers right after electrospinning step for 2 h. The nanofibrous membranes were stored at ambient temperature for 24 h to be dried.

## 2.6. Characterization

### 2.6.1. Solution characterization

The electrical conductivity of spinning solutions was measured using a conductivity meter (OAKLON pH/CON 510 Benchtop Meter). The conductivity electrode was entirely submerged in the solution, and at room temperature, the conductivity measurement was carried out after stabilizing the reader. The viscosity of spinning solutions was determined by a digital viscometer (Brookfield) in a 20 mL cylindrical sample container at a constant solution temperature of 25 °C using an S-31 spindle. The rotation frequency of the S-31 spindle was 50 rpm, and the shear rate was 10.2 S<sup>-1</sup>.

### 2.6.2. Membrane characterization

The morphological structure of CNC/CA and TOCNF/CA composite nanofibers was investigated by a Scanning Electron Microscope (SEM), Hitachi Model S3600-N. The SEM was performed at 5 kV in three magnifications. The SEM samples were coated with gold using a sputter coater (Quorum Technologies - Model K550X) under 35 mA current for 2 min. The fiber distribution and mean fiber diameter size were measured using image processing software (ImageJ, 2.0.0-rc-43/1.50e) based on 40 fibers.

Mechanical properties of samples were measured on a Pneumatic tensile machine (Alliance RF/200(MTS)) at a loading speed of 2 mm/min equipped with a load cell of 100 N. All the ENM samples were measured 70 mm long by 10 mm wide. The upper and lower grips were clamped to the sample at 10 mm. An average value from three replicates was taken for all samples. The room temperature and relative humidity were controlled constant at 25 °C and 50%, respectively.

Fourier transform infrared (FTIR, Perkin Elmer) spect roscopic analysis of all samples was performed with a resolution of 2 cm<sup>-1</sup> by averaging 64 scans in the range of 4000–400 cm<sup>-1</sup>. FTIR of all nanofibrous membranes was taken under an attenuated total reflection (ATR) mode using the corresponding accessory.

## 3. Results and discussion

In this study, CNC/CA and TOCNF/CA solutions composed of 15 wt% CA as matrix polymer and four loadings of CNC or TOCNF nanofillers (i. e., 0.25, 0.5, 0.75, and 1 wt%) in 1:1 volume ratio of DMF and acetone mixture solvent were electrospun. The electrospinning method is used to prepare the composite nanofibrous membranes and study the effects of nanofiller loading and HPT process on the microstructure and mechanical properties of ENMs during constant electrospinning process conditions. The following sections describe the impact of the HPT process, and compare the effects of CNC and TOCNF reinforcing agents on the bead-free morphological structure and accordingly on the mechanical properties of the CA nanocomposite samples.

### 3.1. Conductivity and viscosity of composite spinning solutions

In general, the final morphology of nanofibers is highly affected by several solution parameters such as viscosity and conductivity. Bar graphs in Fig. 3(a) and (b) illustrate the effect of the nanofiller loading on the conductivity and viscosity of the composite spinning solutions, respectively.

At the equal nanofiller loading, the viscosity and conductivity of the TOCNF/CA solutions are higher than CNC/CA solutions. The presence of fibrous molecules in TOCNFs affects CA entanglement, which results in higher viscosity. After TEMPO-mediated oxidation of CNF, surface hydroxyls of cellulose convert into stable charged carboxyl groups. The presence of carboxyl groups in the TOCNF increased the anionicity of the TOCNF, (See Table 2). Hence, higher conductivity of TOCNF/CA solutions is attributed to the stronger ionic interactions between the negatively charged TOCNFs and the positively charged CA chains (Campano

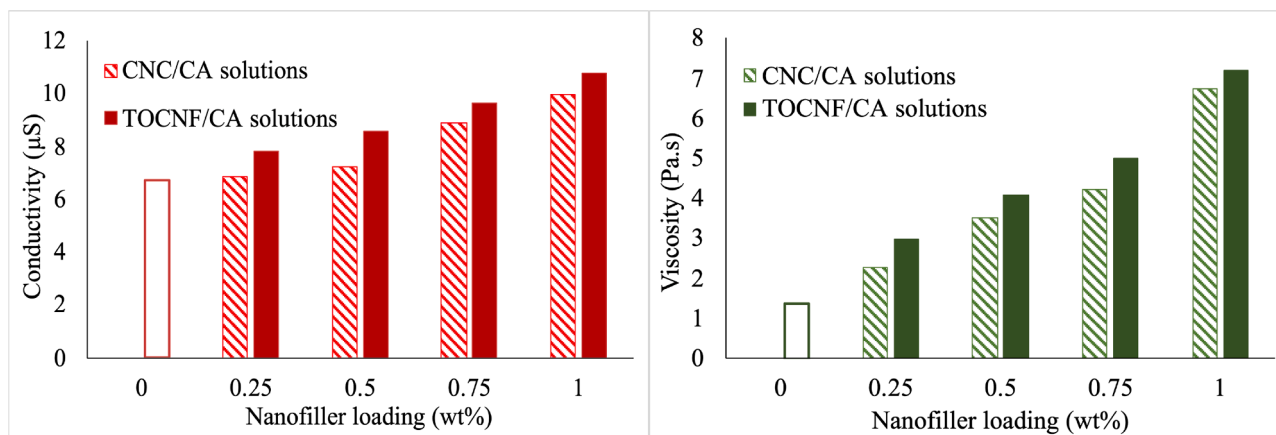


Fig. 3. The impact of CNC/TOCNF loading on a) conductivity and b) viscosity of the spinning solutions.

et al., 2018; Habibi et al., 2006). According to the red and green unfilled and hatched bar graphs in Fig. 3(a) and (b) that belong to the data related to pure CA and CNC/CA spinning solutions, the conductivity and also the viscosity of CNC/CA spinning solutions were increased with the elevation of CNC loading from 0 wt% to 1 wt%. The red and green unfilled and solid bar graphs show the same increasing trend for TOCNF/CA spinning solutions.

### 3.2. Structural effects: HPT process

The SEM micrographs of pristine CA ENMs as-synthesized and after HPT are shown in Fig. 4(a), and (b). These micrographs are visual pieces of evidence that the fiber diameter on average has increased after the HPT process. The subplots in the bottom corner of each micrograph convey the size distribution for the fibers following a normal distribution.

The mean and range of fiber diameters were extracted by image analysis and are reported in Fig. 4(s) and Fig. 4(t), respectively to further elucidate the morphological effects of nanofiller loading and HPT process. The size analysis for pure CA nanofibers shows that the mean fiber diameter has increased from 203 nm to 322 nm after the HPT process and the fiber distribution widened as the fiber diameter range increased from 372 nm to 626 nm.

In addition to pure CA ENMs, the micrographs of nanocomposite CNC/CA and TOCNF/CA ENMs as-synthesized and after HPT are shown in Fig. 4(c) to (r) for different loadings of reinforcing agent additive in the spinning solution. An initial visual inspection of the micrographs reveals an increase in fiber diameter at constant electrospinning process conditions after HPT due to the physical connection of the fibers to each other. Additionally, the mean diameter of the fibers was increased after HPT due to mild melting on the surface (You et al., 2006).

Using image analysis, mean fiber diameter and fiber diameter range of ENM samples were obtained and summarized in Fig. 4(s), and (t). The graphs demonstrate the structural effects of the HPT process. In Fig. 4(s), comparing the dashed and solid red lines to gray ones illustrates the enhancing effect of HPT process on increasing the fiber diameter of both CNC/CA and TOCNF/CA ENMs, respectively. A similar trend for the range of fiber diameter for both types of composite samples is shown in Fig. 4 (t) where the increase in fiber diameter range with the implementation of HPT is clearly evident.

### 3.3. Structural effects: nanofiller loading

The SEM micrographs and corresponding fiber diameter distribution graphs of CNC/CA and TOCNF/CA ENMs for varying loadings from 0 wt% to 1 wt% are shown in Fig. 4 (a) to (r). Visual observation reveals that from the upper graphs toward the bottom graphs, with increasing the

nanofiller loading from 0 wt% to 1 wt%, thicker fibers with a broader diameter range can be obtained. Moreover, the fiber distribution curve tends to be inclined toward larger diameters, which means the density of thicker fibers increases as the nanofiller loading in the spinning solution increases.

Based on the summarized image analysis results in Fig. 4(s), the gray dashed line graph indicates that with increasing CNC loading from 0 wt% to 1 wt%, the mean fiber diameter of nanocomposite CNC/CA ENMs was increased from 203 to 404 nm. The gray solid line graph in Fig. 4(s) shows the changes in mean fiber diameter in terms of loading for TOCNF/CA nanocomposite ENMs. By adding 1 wt% TOCNF to the spinning solution, the mean fiber diameter of the pristine CA ENM sample is increased from 203 to 447 nm. The slope of both dashed and solid gray graphs which are equivalent to the variation rate of mean fiber diameter in relation to nanofiller loading is increased after 0.5 wt% CNC and 0.25 wt% TOCNF. At the same nanofiller loading, the fibrous structure of TOCNF causes higher viscosity in the spinning solution resulting in thicker and broader fiber diameter distribution in TOCNF/CA membranes in comparison to CNC/CA samples. The further addition of reinforcing agents results in a more viscous polymer solution. When the viscosity of the solution is higher, at the same electrospinning process conditions, the polymer spinning solution is more resistant to stretching from the electric field force, resulting in thicker fibers (Jiang et al., 2020). In Fig. 4(t) based on solid bar charts, in addition to the incremental effect of HPT, the increase in nanofiller loading from 0 wt% to 1 wt% has boosted the fiber diameter range from 626 nm to 810 nm and from 626 nm to 841 nm for CNC/CA and TOCNF/CA composite ENMs, respectively.

### 3.4. FTIR spectroscopy

FTIR spectroscopy was used for the investigation of chemical interactions between reinforcing agents and CA in membrane samples. The FTIR spectrums of CNC/CA and TOCNF/CA samples for different loadings of the nanofillers are shown in Fig. 5(a), and (b), respectively. The chemical structure of cellulose nanocrystals and TEMPO-oxidized cellulose nanofibrils are demonstrated in the left corner of Fig. 5(a), and (b), respectively.

It appears that the dominant spectral bands in the wavenumber range of 500–4000  $cm^{-1}$  correspond to the stretching vibrations of C-O and -C=O carboxyl groups from residual acetate groups in the CA matrix at 1031  $cm^{-1}$ , 1218  $cm^{-1}$ , and 1738  $cm^{-1}$ . As seen in Fig. 5 (a), when CNCs were added to the fibers, there was a dramatic increase in the relative intensity of the peaks related to cellulose, such as cellulose's most intense absorption band at 1031  $cm^{-1}$ . The bands near 900  $cm^{-1}$  and 1369  $cm^{-1}$  correspond to the C-H bending vibration of the -CH<sub>3</sub>

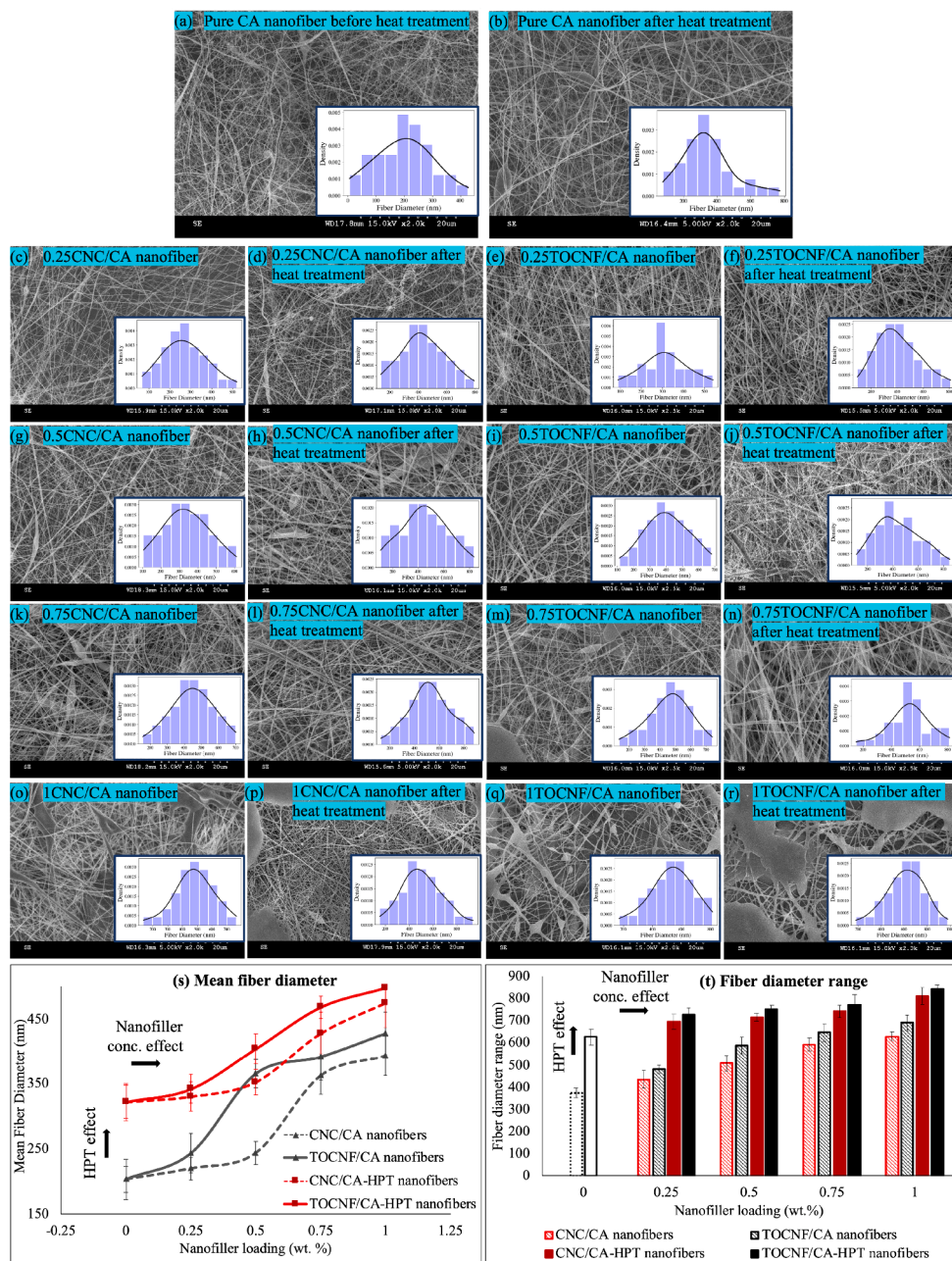


**Fig. 4.** SEM images, fiber diameter distribution and range for pristine CA nanofibers and CNC/CA and TOCNF/CA ENMs as-spun and after HPT process (a)Pristine CA nanofibers as-synthesized (b)Pristine CA nanofibers after HPT (c) to (r) CNC/CA and TOCNF/CA composite nanofibers as-spun and after HPT process (s) Mean fiber diameter vs. nanofiller loading (t)Fiber diameter range vs. nanofiller loading.

group. The peak around  $600\text{ cm}^{-1}$  is the bending vibration of -CH. The presence of a band at  $1639\text{ cm}^{-1}$  due to -OH bending indicates the presence of water in the structure of the nanofibers. A higher loading of nanofiller causes an increase in peak area, which is a result of more -OH vibrations from the adsorption of water. According to Fig. 5(a), and (b), by increasing CNC loading, the absorption peaks became stronger gradually. In contrast for TOCNFs, the absorption peaks are slightly augmented when the nanofiller loading is increased from 0 wt% to 0.75 wt%, with further increases in loading to 1 wt% leading to stronger absorption peaks. This is due to the more challenging distribution and dispersion of fibrous CNFs in the polymer matrix as opposed to CNCs. The small peaks are shown at  $2920\text{ cm}^{-1}$  (-CH stretching vibrations from alkyl groups) and  $3420\text{ cm}^{-1}$  (free -OH stretching vibrations of -OH groups) in the FTIR spectra of 1TOCNF/CA composite ENM. The peak at

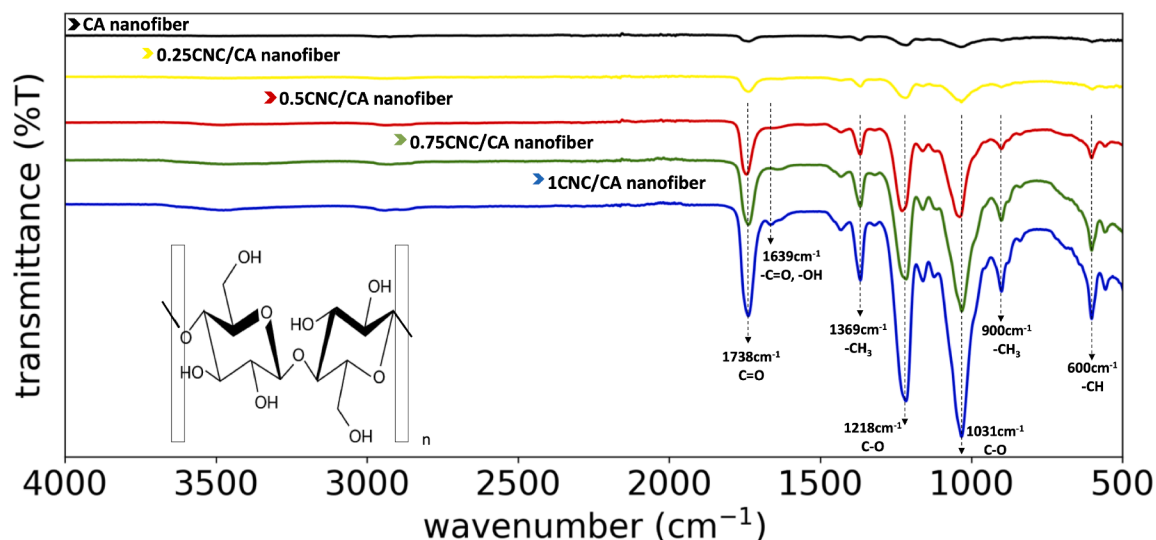
$3420\text{ cm}^{-1}$  indicates the formation of H-bonding between the TOCNF molecule and adsorbed water.

Fig. 6 shows the FTIR spectra acquired from the 0.5CNC/CA ENM samples as-synthesized and after the HPT process. It is evident from the coinciding peaks that the HPT process does not alter the composition of membrane samples.

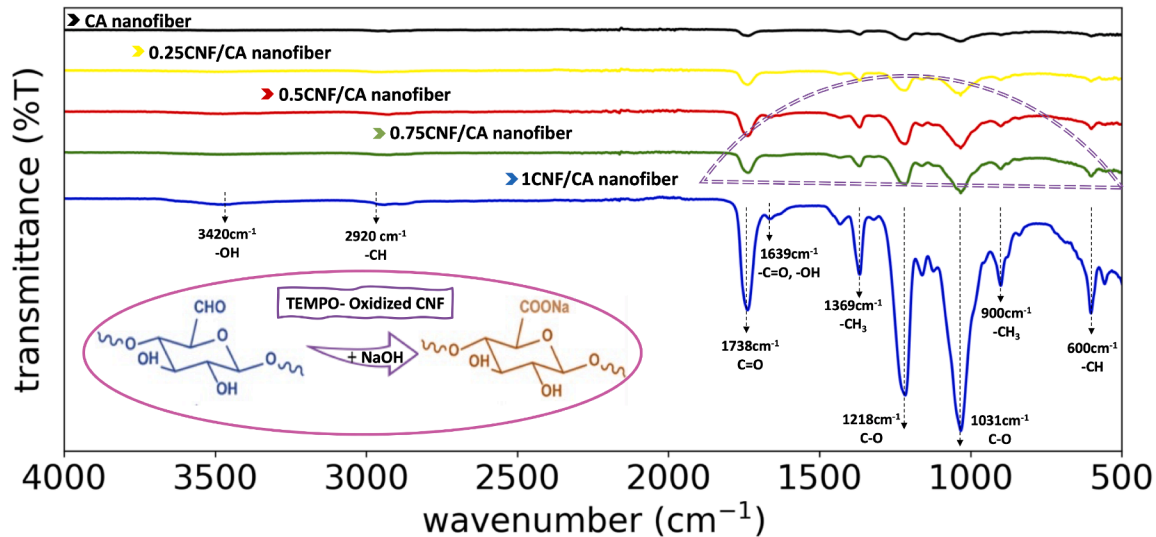
### 3.5. Mechanical properties

The mechanical properties of nanocomposite membrane samples were analyzed to investigate the reinforcing impacts of nanocellulose fillers and the HPT process. Fig. 7(a) and (b) present stress-strain curves for CNC/CA and TOCNF/CA nanocomposite ENMs with different reinforcing agent loadings as-spun and after the HPT process. The mechanical properties of the membranes are summarized in Tables 4 and 5.





(a)



(b)

Fig. 5. FTIR spectra of ENMs (a) CNC/CA composite ENMs (b) TOCNF/CA composite ENMs as-spun (For interpretation of the colors in this figure please refer to the online version of this document.)

The extracted properties include the mean fiber diameter, fiber diameter range, ultimate tensile strength (UTS), elongation at break point, and Young's modulus. In Fig. 7(a) and (b), the solid and dashed lines illustrate the tensile curves for ENM samples prior to and after the HPT process, respectively. During the early stages of straining the as-synthesized samples, i.e., solid lines, there is a great deal of resistance to deformation in the beginning of the tensile test. Based on the results in Tables 4 and 5, as the content of CNC and TOCNF nanofiller increased, Young's modulus reach a maximum of 4.2 GPa and 5.3 GPa for as-spun 0.5CNC/CA and 0.25TOCNF/CA ENMs, respectively. This high resistance with respect to the pure CA ENM sample is because of the large number of fiber-to-fiber connections and the development of collective intermolecular forces within the fiber mass. Due to stronger intermolecular forces in the case of TOCNF/CA composite ENMs, higher deformation resistance was observed in Fig. 7(b) i.e., solid curves. The fiber connections fail more severely in the presence of further deformation,

resulting in a smaller cross-section of the specimen.

The UTS and elongation at break of pristine CA nanofibrous membrane sample prior to HPT process is 5.1 MPa and 0.76%, respectively. By increasing the CNC loading from 0 wt% to 1 wt% in spinning solution, both UTS and fracture strain reach a maximum of 15.4 MPa, and 1.18% at the CNC loading of 0.5 wt% which are 3 times and 1.5 times that of pristine CA membrane, respectively (Fig. 7 (a) i.e., solid curves). Similar works which are introduced CNCs as nanofiller to the structure of nanofibers, only showed 1.4 times (Sun et al., 2015) and 2.2 times (Jiang et al., 2020) improvement in UTS of CNC/CA composite nanofibers in comparison to CA nanofibers (See Table 1). As can be seen in Fig. 7(b), i.e., solid curves, the maximum UTS and fracture strain of 22.6 MPa, and 1.25% are achieved for 0.25TOCNF/CA membrane sample prior to the HPT process which are 4.4 times and 1.6 times those of pristine CA nanofiber membranes, respectively. To the best of authors' knowledge, there are limited studies on electrospun CNF/CA

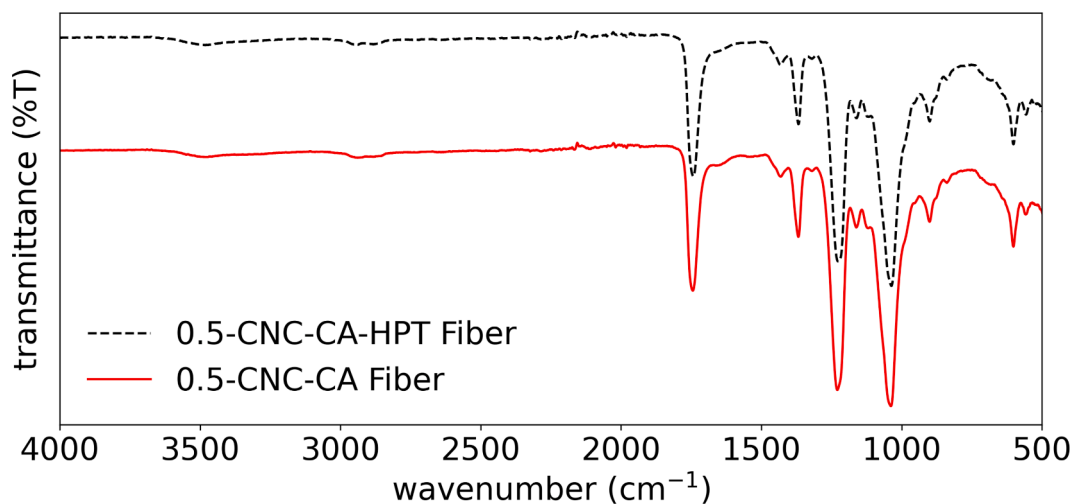


Fig. 6. FTIR spectra of 0.5CNC/CA electrospun nanofibrous membrane samples as-spun and after HPT process

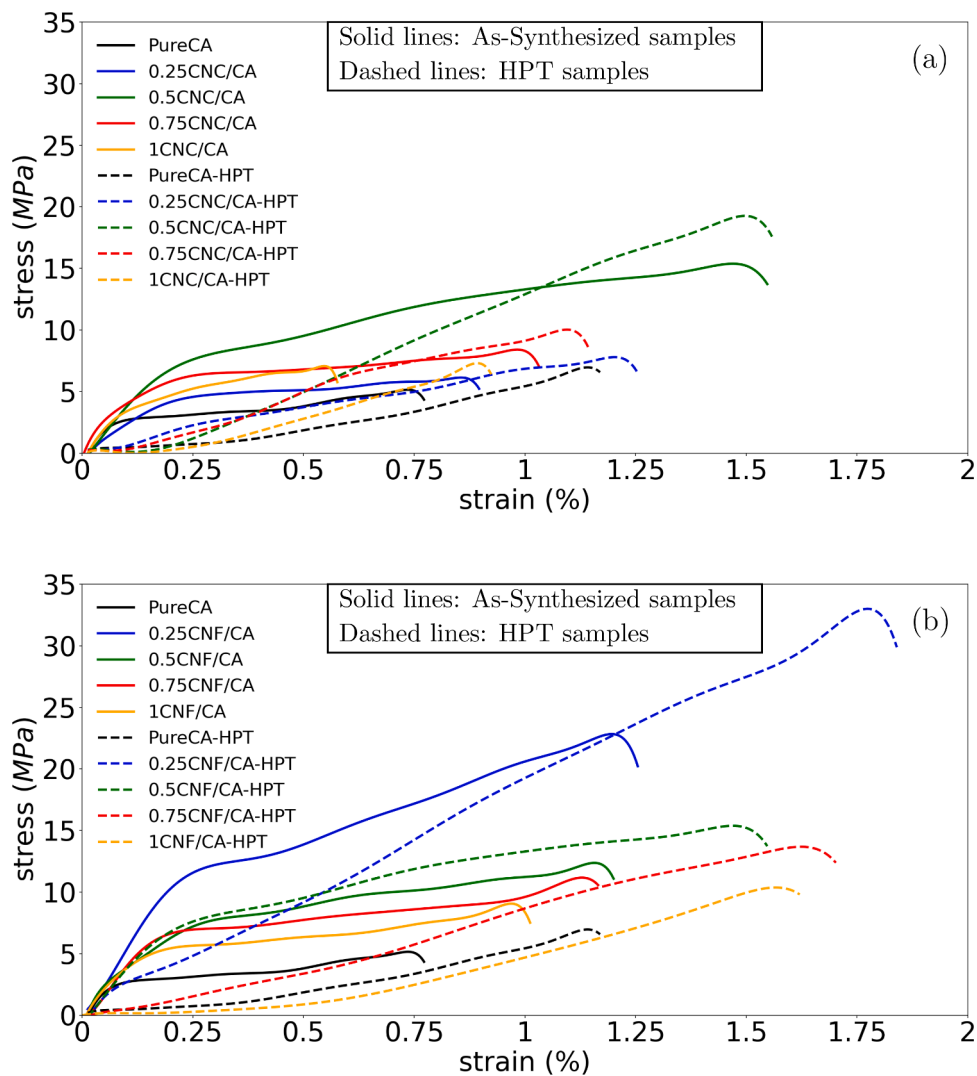


Fig. 7. The effect of (a) CNC and (b) TOCNF nanofillers on mechanical properties of CA ENMs as-spun and after HPT process (For interpretation of the colors in this figure please refer to the online version of this document.).

**Table 4**

The mechanical properties of CNC/CA nanocomposite ENMs.

Sample Code	CA		0.25CNC/CA		0.5CNC/CA		0.75CNC/CA		1CNC/CA	
	AS*	HPT*	AS	HPT	AS	HPT	AS	HPT	AS	HPT
Mean Diameter(nm)	203±20	322±24	219±17	330±23	243±18	352±20	362±28	428±32	404±21	474±19
Diameter Range(nm)	372±22	626±35	434±38	694±33	507±36	716±18	592±30	741±27	629±19	810±38
UTS(MPa)	5.1±0.9	7.2±1.5	6.1±0.8	8±0.9	15.3±1.2	19.7±0.7	8.4±1.4	10.2±1	6.3±0.6	7.6±1.6
Strain at Break(%)	0.76±0.11	1.17±0.32	0.89±0.21	1.22±0.31	1.54±0.38	1.55±0.35	1.02±0.26	1.13±0.27	0.57±0.09	0.91±0.11
Modulus(GPa)	1.13±0.21		1.6±0.17		4.2±0.51		3.4±0.33		1.8±0.19	

★ AS: As-Synthesized, HPT: After Heat Treatment Process.

**Table 5**

The mechanical properties of TOCNF/CA composite ENMs.

Sample Code	CA		0.25CNF/CA		0.5CNF/CA		0.75CNF/CA		1CNF/CA	
	AS*	HPT*	AS	HPT	AS	HPT	AS	HPT	AS	HPT
Mean Diameter(nm)	203±20	322±24	233±30	342±22	345±22	404±23	411±35	468±17	447±31	498±13
Diameter Range(nm)	372±22	626±35	480±18	727±28	587±37	749±19	646±40	772±45	690±35	841±20
UTS(MPa)	5.1±0.9	7.15±1.5	22.6±1.9	33.31±1.3	12.5±1.7	16.4±0.6	11.4±1	13.97±0.8	8.99±0.7	10.46±0.4
Strain at Break(%)	0.76±0.11	1.17±0.32	1.25±0.27	1.83±0.41	1.19±0.17	1.54±0.19	1.17±0.22	1.69±0.35	0.99±0.13	1.61±0.48
Modulus(GPa)	1.13±0.21		5.3±1.69		3.5±1.08		2.7±0.79		1.5±0.58	

★ AS: As-Synthesized, HPT: After Heat Treatment Process.

nanocomposite membranes and their mechanical properties. The CNF/CA nanocomposite membranes synthesized by Sharma et al. (2021) and Cindradewi et al. (2021) are obtained using phase inversion methods and do not exhibit a nanofibrous structure. As a result, the UTS of their samples is 65 MPa and 47.6 MPa, respectively, which is due to the dense and bulk structure of the membranes. (See Table 1).

Fig. 7 (a) and (b) reflect similarities between the tensile strength of CNC/CA and TOCNF/CA ENMs. Both types of CNC/CA and TOCNF/CA ENMs illustrate that by increasing the nanofiller loading in spinning solution and consequently mean fiber diameter, the tensile strength after reaching a maximum value for 0.5CNC/CA and 0.25TOCNF/CA ENMs eventually falls off with a further increase in the nanofiller loading. According to Fig. 4 (s), the slope of the gray dashed curve and the gray solid curve have been sharpened after 0.5 wt% CNC and 0.25 wt% TOCNF for CNC/CA and TOCNF/CA composite nanofibers, respectively. This increasing trend may indicate the maximum value of stress and also an inverse correlation between mean fiber diameter and the tensile strength of nanocomposite membranes. It could be explained by a decrease in fiber connections due to increased fiber diameters, which in turn led to a decrease in fiber length at the same membrane area density. Meanwhile, the possible aggregation of the nanofillers could be responsible for the decrease in tensile strength with further nanofiller loading. According to Fig. 7 (a) and (b), the decrease in tensile strength due to the increase in TOCNF loading above 0.25 wt% is higher than in the case of CNCs. Possibly, TOCNFs aggregate more readily and form stronger hydrogen bonds than CNCs. The mechanical properties of ENMs are strongly influenced by how nanofillers are distributed and dispersed throughout their structure. The reinforcement effect of CNCs and TOCNFs is responsible for the considerable improvement in fracture strength of composite nanofibrous membranes. Nanocomposites containing TOCNFs have higher tensile strength than those containing CNCs, likely due to the stronger ionic interaction between the negatively charged TOCNFs and positively charged CA chains. Further, it may be rooted in the fibrous structure of TOCNFs, resulting in greater interaction and cross-linking with the CA matrix. The dashed curves in the Fig. 7 (a) and (b) illustrates how the HPT process affects the mechanical properties of the CNC/CA, and TOCNF/CA composite nanofibers in different nanofiller loadings. As depicted in Fig. 7 (a) and (b), thermally treated nanocomposite membranes exhibited remarkably different stress-strain behavior than the samples prior to the HPT process. In the

process of heat treating, the yield points almost faded away, resulting in a linear behavior. These results reflect that the heat-treated samples have together tougher, stronger, and more coherent structures. Based on the results, the improvement in both UTS and fracture strain after heat treatment was observed. The bonding between nanofibers is mainly caused by cross-linking between nanofibers after heat treatment. Furthermore, heat treatment can improve membrane integrity by removing solvents from nanofibers.

Fig. 8 shows the comparisons of UTS among pristine CA nanofibers, CNC nanofiller-reinforced CA composite ENMs, and TOCNF nanofiller-reinforced CA composite ENMs as a function of nanofiller loadings and HPT process. Overall, the addition of CNC and TOCNF reinforcements to the CA matrix results in the elevation of tensile strength. The maximum UTS of 33.31 MPa and maximum elongation at break point of 1.83% was obtained for heat treated 0.25TOCNF/CA composite ENM sample. The addition of TOCNFs improves the flexibility of TOCNF/CA composite ENM sample by the formation of good interfacial bonding between the CA matrix and the fibrils (Liu et al., 2013; Wu et al., 2019). Based on Fig. 8, by further increasing of TOCNF weight percentage from 0.25 wt% to 1 wt% in the polymer spinning solution the tensile strength is decreased. This decreasing tendency might be caused by the inhomogeneous distribution of TOCNF nanofiller in the CA polymer matrix, caused by the high aspect ratio of TOCNFs, and the formation of aggregations that occurred by strong hydrogen bonds and swollen clusters by water in the solution.

#### 4. Conclusion

In this study, the effect of reinforcing nanofillers and subsequent heat post-treatment on the integrity and mechanical properties of Cellulose acetate (CA)-based membranes were investigated. Various CA electrospun nanofibrous membrane (ENM) samples were prepared by modifying the loading (i.e., 0.25, 0.5, 0.75, 1 wt%) and type of nanofiller reinforcements (i.e., Cellulose nanocrystal (CNC), Tempo-oxidized cellulose nanofibril(TOCNF)) while keeping the other material and process parameters (i.e., CA concentration and several electrospinning process parameters) constant. We chose CA concentration at the optimized value of 15 wt%, the polymer flow rate of 2 ml/h, tip-to-collector distance of 100 mm, and electric voltage of 25 kV for 2 h of the spinning process (refer to Ref. Attari and Hausler, 2020 for optimization). Structural and



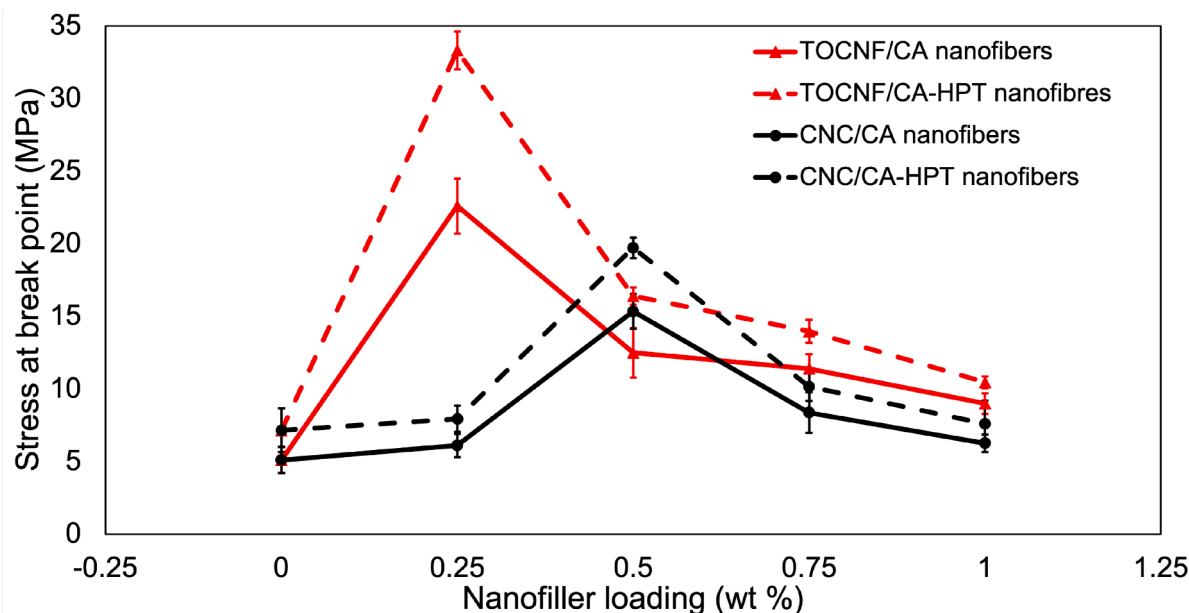


Fig. 8. Variations of tensile strength of CNC/CA and TOCNF/CA ENMs as a function of nanofiller loading and heat treatment process (For interpretation of the colors in this figure please refer to the online version of this document.).

mechanical properties of the membrane samples were characterized by SEM, imageJ, FTIR, and tensile analyses. According to SEM and ImageJ analysis, the nanocelluloses/CA electrospun fibers were smooth and bead-free, and their mean fiber diameter was strongly affected by nanofiller loading and heat treatment. As CNC and TOCNF loading increased in polymer spinning solution, single fibers in ENM samples got thicker resulting in larger mean fiber diameters. Likewise, after heat post-treatment, ENM samples exhibited increased mean fiber diameter. FTIR analysis indicated that hydrogen bonds were formed between TOCNF molecules and adsorbed water. In terms of mechanical properties, mean fiber diameter and tensile strength are correlated. A decrease in tensile strength was observed with an increase in mean fiber diameter. Maximum UTS of 33.3 MPa and elongation at break of 1.83% were achieved for heat-treated 0.25TOCNF/CA ENM sample, which represents 6.5 times and 2.5 times greater than those obtained for pristine CA ENM sample. According to our study, TOCNF nanofillers had superior reinforcement properties compared to CNC nanofillers due to their fibrous structure and also TEMPO-mediated surface oxidation. All these results are proof of the possibility of controlling the structure of the CA ENMs using an effective procedure for achieving the desired morphology. Process-structure-property chain relationship outlined in this study is a prominent step in designing and integrating membrane technology into the water remediation processes.

#### Declaration of Competing Interest

The authors declare that they have no known competing financial interests or personal relationships that could have appeared to influence the work reported in this paper.

#### Data availability

Data will be made available on request.

#### Acknowledgment

Nasrin Attari is thankful to Arbour Foundation, Molson Foundation, and École de technologie supérieure for their separate financial support and fellowships that made this research possible. Part of this research

has been carried out in the STEPPE and material characterization Laboratories of ETS University. Also, NA gratefully acknowledges the support from Dr. Martha Cerruti, the head of the Biointerface Laboratory of McGill University for providing electrospinning equipment to carry out the research reported in this article.

#### References

- Abdullah, N., Yusof, N., Lau, W. J., Jaafar, J., & Ismail, A. F. (2019). Recent trends of heavy metal removal from water/wastewater by membrane technologies. *Journal of Industrial and Engineering Chemistry*, 76, 17–38.
- Aboamara, N. M., Mohamed, A., Salama, A., Osman, T. A., & Khattab, A. (2019). Characterization and mechanical properties of electrospun cellulose acetate/graphene oxide composite nanofibers. *Mechanics of Advanced Materials and Structures*, 26(9), 765–769.
- Aruchamy, K., Mahto, A., & Nataraj, S. K. (2018). Electrospun nanofibers, nanocomposites and characterization of art: insight on establishing fibers as product. *Nano-Structures & Nano-Objects*, 16, 45–58.
- Attari, N., & Hausler, R. (2020). Morphological investigation of cellulose acetate nanofibrous membranes. Proceedings of the 4rd international conference of recent trends in environmental science and engineering (RTESE'20).
- Babaei-Ghazvini, A., & Acharya, B. (2022). Influence of cellulose nanocrystal aspect ratio on shear force aligned films: Physical and mechanical properties. *Carbohydrate Polymer Technologies and Applications*, 3, 100217.
- Bay, R. K., Zarybnicka, K., Jancar, J., & Crosby, A. J. (2020). Mechanical properties of ultrathin polymer nanocomposites. *ACS Applied Polymer Materials*, 2(6), 2220–2227.
- Cai, S., Li, Y., Liu, H.-Y., & Mai, Y.-W. (2019). Effect of electrospun polysulfone/cellulose nanocrystals interleaves on the interlaminar fracture toughness of carbon fiber/epoxy composites. *Composites Science and Technology*, 181, 107673.
- Campano, C., Merayo, N., Balea, A., Tarrés, Q., Delgado-Aguilar, M., Mutjé, P., Negro, C., & Blanco, A. (2018). Mechanical and chemical dispersion of nanocelluloses to improve their reinforcing effect on recycled paper. *Cellulose*, 25(1), 269–280.
- Cindradewi, A. W., Bandi, R., Park, C.-W., Park, J.-S., Lee, E.-A., Kim, J.-K., Kwon, G.-J., Han, S.-Y., & Lee, S.-H. (2021). Preparation and characterization of cellulose acetate film reinforced with cellulose nanofibril. *Polymers*, 13(17), 2990.
- Del Río De Vicente, J. I. (2021). Cellulose nanocrystals functionalized cellulose acetate electrospun membranes for adsorption and separation of nanosized particles.
- Divya, S., & Oh, T. H. (2022). Polymer nanocomposite membrane for wastewater treatment: A critical review. *Polymers*, 14(9), 1732.
- Etemadi, H., Yegani, R., & Babaeipour, V. (2016). Study on the reinforcing effect of nanodiamond particles on the mechanical, thermal and antibacterial properties of cellulose acetate membranes. *Diamond and Related Materials*, 69, 166–176.
- Fane, A. G., Wang, R., & Jia, Y. (2011). *Membrane technology: past, present and future*. Springer.
- Fischer, S., Thümmel, K., Volkert, B., Hettrich, K., Schmidt, I., & Fischer, K. (2008). Properties and applications of cellulose acetate, vol. 262. *Macromolecular symposia* (pp. 89–96). Wiley Online Library.
- Gaitán, A., & Gacitúa, W. (2018). Morphological and mechanical characterization of electrospun polylactic acid and microcrystalline cellulose. *BioResources*, 13(2), 3659–3673.

- Ghasemi, S., Behrooz, R., Ghasemi, I., Yassar, R. S., & Long, F. (2018). Development of nanocellulose-reinforced PLA nanocomposite by using maleated PLA (PLA-g-MA). *Journal of Thermoplastic Composite Materials*, 31(8), 1090–1101.
- Goetz, L. A., Naseri, N., Nair, S. S., Karim, Z., & Mathew, A. P. (2018). All cellulose electrospun water purification membranes nanotextured using cellulose nanocrystals. *Cellulose*, 25(5), 3011–3023.
- Habibi, Y., Chanzy, H., & Vignon, M. R. (2006). Tempo-mediated surface oxidation of cellulose whiskers. *Cellulose*, 13(6), 679–687.
- Janeca, A., Rodrigues, F. S. C., Gonçalves, M. C., & Faria, M. (2021). Novel cellulose acetate-based monophasic hybrid membranes for improved blood purification devices: Characterization under dynamic conditions. *Membranes*, 11(11), 825.
- Jiang, L., Li, K., Yang, H., Liu, X., Li, W., Xu, W., & Deng, B. (2020). Improving mechanical properties of electrospun cellulose acetate nanofiber membranes by cellulose nanocrystals with and without polyvinylpyrrolidone. *Cellulose*, 27(2), 955–967.
- Jonoobi, M., Harun, J., Mathew, A. P., & Oksman, K. (2010). Mechanical properties of cellulose nanofiber (CNF) reinforced polylactic acid (PLA) prepared by twin screw extrusion. *Composites Science and Technology*, 70(12), 1742–1747.
- Kugarajah, V., Ojha, A. K., Ranjan, S., Dasgupta, N., Ganesapillai, M., Dharmalingam, S., Elmoll, A., Hosseini, S. A., Muthulakshmi, L., Vijayakumar, S., et al. (2021). Future applications of electrospun nanofibers in pressure driven water treatment: A brief review and research update. *Journal of Environmental Chemical Engineering*, 9(2), 105107.
- Lalia, B. S., Guillen, E., Arafat, H. A., & Hashaikeh, R. (2014). Nanocrystalline cellulose reinforced PVDF-HFP membranes for membrane distillation application. *Desalination*, 332(1), 134–141.
- Lee, H., Nishino, M., Sohn, D., Lee, J. S., & Kim, I. S. (2018). Control of the morphology of cellulose acetate nanofibers via electrospinning. *Cellulose*, 25(5), 2829–2837.
- Levanic, J., Šenk, V. P., Nadrah, P., Poljanšek, I., Oven, P., & Haapala, A. (2020). Analyzing TEMPO-oxidized cellulose fiber morphology: new insights into optimization of the oxidation process and nanocellulose dispersion quality. *ACS Sustainable Chemistry & Engineering*, 8(48), 17752–17762.
- Liu, D., Sun, X., Tian, H., Maiti, S., & Ma, Z. (2013). Effects of cellulose nanofibrils on the structure and properties on PVA nanocomposites. *Cellulose*, 20(6), 2981–2989.
- Liu, H., & Tang, C. (2007). Electrospinning of cellulose acetate in solvent mixture n, n-dimethylacetamide (DMAc)/acetone. *Polymer journal*, 39(1), 65–72.
- Ma, H., Burger, C., Hsiao, B. S., & Chu, B. (2014). Fabrication and characterization of cellulose nanofiber based thin-film nanofibrous composite membranes. *Journal of Membrane Science*, 454, 272–282.
- Patiño Masó, J., Serra-Parareda, F., Tarrés, Q., Mutjé, P., Espinach, F. X., & Delgado-Aguilar, M. (2019). Tempo-oxidized cellulose nanofibers: a potential bio-based superabsorbent for diaper production. *Nanomaterials*, 9(9), 1271.
- Mokhena, T. C., Jacobs, N. V., & Luyt, A. S. (2018). Nanofibrous alginate membrane coated with cellulose nanowhiskers for water purification. *Cellulose*, 25(1), 417–427.
- Nasir, A., Masood, F., Yasin, T., & Hameed, A. (2019). Progress in polymeric nanocomposite membranes for wastewater treatment: Preparation, properties and applications. *Journal of Industrial and Engineering Chemistry*, 79, 29–40.
- Patterson, J. W. (1985). *Industrial wastewater treatment technology*. Butterworth Publishers, Stoneham, MA.
- Pinnau, I., & Freeman, B. D. (2000). *Formation and modification of polymeric membranes: overview*. ACS Publications.
- Quebec Ministry of the Environment. (1995). *25 years of industrial wastewater treatment in Quebec - report*. Les Publications du Quebec.
- Salama, A., Mohamed, A., Aboamra, N. M., Osman, T., & Khattab, A. (2018). Characterization and mechanical properties of cellulose acetate/carbon nanotube composite nanofibers. *Advances in Polymer Technology*, 37(7), 2446–2451.
- Sharma, A., Mandal, T., & Goswami, S. (2021). Fabrication of cellulose acetate nanocomposite films with lignocellulosic nanofiber filler for superior effect on thermal, mechanical and optical properties. *Nano-Structures & Nano-Objects*, 25, 100642.
- Stamatialis, D. F., Papenburg, B. J., Gironés, M., Saiful, S., Bettahalli, S. N. M., Schmitmeier, S., & Wessling, M. (2008). Medical applications of membranes: Drug delivery, artificial organs and tissue engineering. *Journal of Membrane Science*, 308 (1-2), 1–34.
- Suja, P. S., Reshmi, C. R., Sagitha, P., & Sujith, A. (2017). Electrospun nanofibrous membranes for water purification. *Polymer reviews*, 57(3), 467–504.
- Sun, C., Boluk, Y., & Ayranci, C. (2015). Investigation of nanofiber nonwoven meshes produced by electrospinning of cellulose nanocrystal suspensions in cellulose acetate solutions. *Cellulose*, 22(4), 2457–2470.
- Vaidya, R., & Wilkins, E. (1994). Effect of interference on amperometric glucose biosensors with cellulose acetate membranes. *Electroanalysis*, 6(8), 677–682.
- Voisin, H., Bergström, L., Liu, P., & Mathew, A. P. (2017). Nanocellulose-based materials for water purification. *Nanomaterials*, 7(3), 57.
- Wang, D., Cheng, W., Wang, Q., Zang, J., Zhang, Y., & Han, G. (2019a). Preparation of electrospun chitosan/poly (ethylene oxide) composite nanofibers reinforced with cellulose nanocrystals: Structure, morphology, and mechanical behavior. *Composites Science and Technology*, 182, 107774.
- Wang, X., Cheng, W., Wang, D., Ni, X., & Han, G. (2019b). Electrospun polyvinylidene fluoride-based fibrous nanocomposite membranes reinforced by cellulose nanocrystals for efficient separation of water-in-oil emulsions. *Journal of Membrane Science*, 575, 71–79.
- Wen, Y., Yuan, J., Ma, X., Wang, S., & Liu, Y. (2019). Polymeric nanocomposite membranes for water treatment: a review. *Environmental Chemistry Letters*, 17(4), 1539–1551.
- Wilderer, P. A. (2010). *Treatise on water science*. Newnes.
- Wsoo, M. A., Shahir, S., Mohd Bohari, S. P., Nayan, N. H. M., & Razak, S. I. A. (2020). A review on the properties of electrospun cellulose acetate and its application in drug delivery systems: A new perspective. *Carbohydrate Research*, 491, 107978.
- Wu, Y., Tang, Q., Yang, F., Xu, L., Wang, X., & Zhang, J. (2019). Mechanical and thermal properties of rice straw cellulose nanofibrils-enhanced polyvinyl alcohol films using freezing-and-thawing cycle method. *Cellulose*, 26(5), 3193–3204.
- You, Y., Lee, S. W., Lee, S. J., & Park, W. H. (2006). Thermal interfiber bonding of electrospun poly (L-lactic acid) nanofibers. *Materials Letters*, 60(11), 1331–1333.
- Zhou, Z., Lin, W., & Wu, X.-F. (2016). Electrospinning ultrathin continuous cellulose acetate fibers for high-flux water filtration. *Colloids and Surfaces A: Physicochemical and Engineering Aspects*, 494, 21–29.